An Enhanced Large-Power *S*-band Injection-Locked Magnetron with Anode Voltage Ripple Inhibition

Xiaojie Chen[1], Bo Yang[2], Xiang Zhao[1], Naoki Shinohara[2], and Changjun Liu[1]
[1]School of Electronics and Information Engineering, Sichuan University, China
[2]Research Institute for Sustainable Humanosphere, Kyoto University, Japan
cjliu.ieee.org, shino@rish.kyoto-u.ac.jp

***Abstract*— A large-power injection-locked magnetron with the anode voltage ripple inhibition was theoretically and experimentally investigated. The enhancement of injection-locking properties of a 20-kW magnetron was presented when the anode voltage ripple is varied from 4.2% to 0.6%. With the improved anode voltage ripple, phase-locking behavior of the magnetron is easier to achieve at lower injection levels and a nearly tripled locking bandwidth was observed. The phase of the magnetron has been precisely locked with a phase jitter of ±0.9°. Furthermore, the spectral intensity increased 0.9 dB at the synchronized frequent point due to the spurious energy suppression. The anode voltage ripple inhibition technique provides guidance for future application of large-power amplifier and phase-controlled arrays based on magnetrons.**

***Keywords*—Anode voltage ripple, phase-locked magnetron, locking bandwidth, spurious suppression.**

I. INTRODUCTION

Space solar power stations (SSPSs) [1], microwave sintering of powdered metals [2], and other technological innovations rely on promising high-power microwave technologies that enable energy savings and emission reduction. The magnetron is a widely-used type of power device that offers high power capacity, high efficiency, and low cost. However, self-oscillated magnetrons cannot be applied directly in phase-controlled applications because of their random phase fluctuations and wide spectral bands [3]. Furthermore, various electrical devices are vulnerable within the frequency range of the extensively applied *S*-band magnetrons; e.g., Zigbee sensors, Bluetooth equipment, Wi-Fi communication devices, and other systems that conform to IEEE 802.11 b/g/n are at high risk of electromagnetic interference from magnetrons.

Therefore, overcoming the problems of the noisy microwave output of a magnetron has attracted significant research attention when the device is selected for use as a microwave source. Mitani *et al*. [4] respectively proposed turning off the filament current and cathode shield technique to improve self-oscillated output quality of a magnetron by reduce the redundancy electrons. Neculaes *et al*. [5] proposed the axially asymmetric azimuthal magnetic field variation method in ovens and in relativistic magnetrons, in which the noises near the carrier frequency are suppressed significantly.

Another widely applied method involves the application of injection locking to a magnetron to solve the unstable output in terms of both phase and frequency, the typical experimental system is shown in Fig. 1. A reference signal injects into a self-oscillated magnetron via a circulator. The magnetron's output will be synchronized with the reference signal when locking occurs. To the applications of injection-locked magnetron, many works were demonstrated in recent years. Shinohara [6] successfully proposed the power-variable phase-controlled magnetron technique, which is intended to be applied to an SSPS source array, using injection locking and phase-locked loop feedback to the anode current. Dexter *et al*. [7] first demonstrated that the single-cell superconducting cavity of a particle accelerator could be driven precisely using a phase-locked magnetron. Modulated signals were achieved by injection locking of magnetrons for communications applications by Yang *et al* [8]. Liu *et al*. [9] concentrated on high-efficiency coherent power combining based on a multi-path phase-locked magnetron to satisfy the increasing demand for power from the microwave industry. Therefore, it is important to improve the output characteristics of phase-locked magnetrons to achieve a wider locking bandwidth and a stable phase output. Such magnetrons are expected to satisfy more applications and reduce any electromagnetic interference in the adjacent channels.

This work presents an approach to improve magnetron's output performance by smoothing its anode voltage, includes

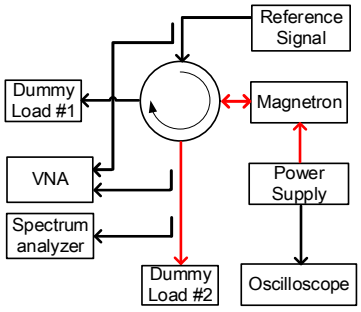

Fig. 1. The block diagram of a phase-locked magnetron system.

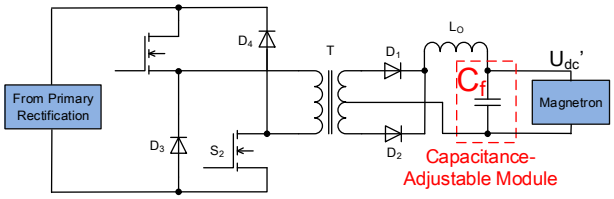

Fig. 2. The simplified schematic of a power supply.

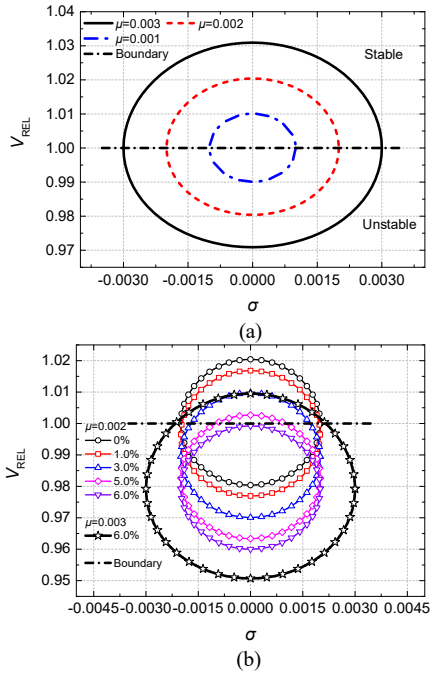

Fig. 3. Theoretical phase-locking performance of magnetron: (a) with various values of injection parameter σ, (b) with respect to the anode voltage ripple S.

theoretical analysis and experimental verification .This is the first time that the correlation between the output of a high-power magnetron and the anode voltage ripples has been demonstrated. In the experiment of a 20 kW S-band phase-locked continuous wave (CW) magnetron, a nearly tripled locking bandwidth, an increment of locking spectral intensity of 0.9 dB and a convergence of phase jitter are respectively obtained when the anode voltage ripple is varied from 4.2% to 0.6%.

II. Numerical Model

A. Governing Equations

In general, the phase-locking state can be illustrated by the classical Adler's condition [10], which is read as

$$\frac{\rho\omega_0}{2Q_e} \geq \Delta\omega \tag{1}$$

where $\rho = (P_{in}/P_0)^{1/2}$ is the injection ratio, Q_e is the external loaded quality factor, $\Delta\omega$ is locking bandwidth, respectively. To investigate the performance of the phase-locked magnetron which is activated by a fluctuated anode voltage, as depicted in Fig.2, the anode voltage is brought by rectification and non-ideal smoothness. We assume that its anode voltage consists of the constant DC voltage U_{dc} and the comparatively slow fluctuation $\Delta U(t)$:

$$U_{dc}' = U_{dc} + \Delta U(t) . \tag{2}$$

Because of its slowly-varying characteristic and the diverse range of ripples caused by the various types of power supply, we believe that the anode voltage with fluctuating components can be regarded as a root mean square (RMS) voltage, and (2) is then modified to read

$$U_{dc}' = U_{dc}\left(1+\frac{R}{2\sqrt{2}}\right) \tag{3}$$

where R is the ripple parameter determined using $R = U_{p\text{-}p}/U_{dc}$, where $U_{p\text{-}p}$ is the peak-to-peak value of the fluctuation. Substitute (3) into the previously deduced locking amplitude-bandwidth equation whose detail derivation isn't presented in this paper, then we obtain:

$$\frac{\left\{U_{REL}\Big/\left[1+R\Big/\left(2\sqrt{2}\right)\right]-1\right\}^2}{\left(\mu/\gamma\right)^2}+\left(\frac{\sigma}{\mu}\right)^2 = 1 \tag{4}$$

where γ is defined as a growth parameter, $U_{REL} = U_{MW}/U_{MW0}$ represents the relative voltage of the locking and self-oscillated outputs, $\mu = \rho/2Q_e$ represents the injection amplitude, and $\sigma = \Delta\omega/\omega_0$ represents the relative locking bandwidth and suggests that all frequencies are normalized with respect to ω_0. Equation (4) describes both the amplitude and the bandwidth of a phase-locked magnetron with respect to its anode voltage ripple.

B. Analysis of Phase-Locked Magnetron with Various Anode Voltage Ripple

To aid in the theoretical analysis, ω_0 is defined to have a constant value of 1. Based on the results suggested by Woo, the typical values of γ/ω_0 range between 0.1 and 0.167 [11]. Therefore, we select the value of $\gamma/\omega_0 = 0.1$ for analysis.

We first consider that anode voltage ripple is evaded, the curves of U_{REL} with respect to σ are shown in Fig. 3 (a). Each curve is plotted with respect to an injection amplitude. All ellipses of locking status have a common geometric center, e.g., $\sigma = 0$ and $U_{REL} = 1$, which represents the self-oscillation condition. Each ellipse can be divided into two parts. The boundary is determined by $U_{REL} = 1$, as indicated by the short-dash-dotted line. If the phase-locked magnetron operates at the upper branch with $U_{REL} > 1$, which is consistent with reality so called stability condition. Otherwise, if there is a negative solution to (4) like that on the lower branch, then the operating condition is not satisfied. The injection amplitude μ in our simulation varies from 0.001 to 0.003 with intervals of 0.001. The locking bandwidth σ in the stable state is represented by two symmetrical points where the ellipse intersects with the boundary line $U_{REL} = 1$. Besides, the anode voltage with zero ripple will lead to the maximum locking bandwidth, which is the prediction of Adler's equation as well.

When the injection amplitude increases, the locking bandwidth extends to become wider and the output power also rises. Additionally, the maximum output voltage is obtained when the injected locking signal has a zero frequency deviation ($\sigma = 0$). When the frequency deviation is equal or greater than μ, no locking status can be achieved.

To analyze the effects of the anode voltage ripple on the magnetron locking condition, we set several reasonable ripples of around 5.0% to analyze the device performance. The effects of the ripple parameter S on the locking results are illustrated in Fig. 3 (b), where the anode voltage ripple parameter S has values of 1.0%, 3.0%, 5.0% and 6.0%, while the injection amplitude remains at $\mu = 0.002$. The stable branches are used to

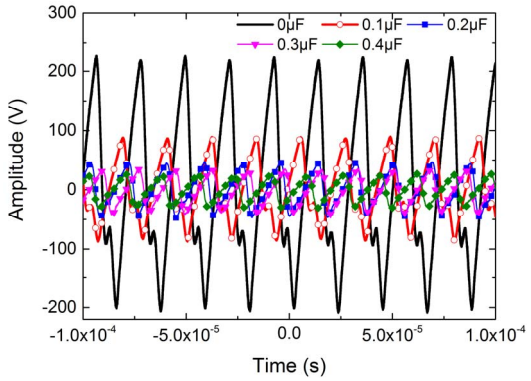

Fig. 4. The measured ripple waveforms with respect to the various filtering capacitances.

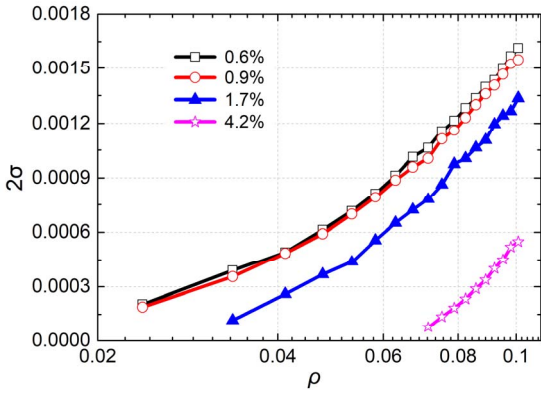

Fig. 5. The measured locking bandwidths of the magnetron for various anode voltage ripples.

evaluate the magnetron's locking performance with respect to the anode voltage ripple. When the ripple varies from 0% to 5.0%, the stable branch moves downward. The magnetron's output voltage at the locking condition has also decreased because of the ripples. When the anode voltage ripple reaches 5.0%, the phase-locking condition may be achieved using only a small-σ injection near the central frequency of the self-oscillated magnetron. However, when the ripple reaches 6.0%, the state ellipse has no intersections with the boundary line where $U_{REL} = 1$. This implies that the magnetron is operating in the unstable region and no phase-locking may be achieved.

Additionally, the performance deterioration caused by the anode voltage ripples can be significantly overcome by increasing the injection amplitude μ to 0.003, as also shown in Fig. 3 (b). However, this may cause the cost of the injection sub-system to rise greatly and is not recommended for the industrial applications.

III. Experimental Analysis and Discussion

A. Experiment Setup

The experimental system block diagram is shown in Fig. 1. The magnetron (CK-2091, Sanle Microwave Co.) is driven by a DC power supply, and its simplified schematic is presented in Fig. 2. It provides a magnetic field intensity of 1250 Gs and a DC anode voltage of 10.4 kV. The DC filament current varies from 47 A to 25 A as the magnetron output power is varied, and it was experimentally proved that the filament current below 30 A no longer has an impact on the phase stability of the magnetron [12]. We intend to control the ripple of the high voltage supply actively to mimic various high voltage supplies with different ripple levels. Therefore, an adjustable capacitance module that is composed of several thin-film capacitors (SDD 20000 V, 0.10 μF, Eaco) is arranged in parallel to filter the ripples. An oscilloscope (DPO-7254, Tektronix) is used to measure the anode voltage ripple via a high-voltage probe (HVP-15HF, 30 dBc, Pinteck). A reference signal is generated by a signal generator (HMC- T2220, Hittite) and amplified using a power amplifier (YYPA4D, Sanle Microwave Co.). At the same time, the time-varied phases, spectra and the power are measured using a vector network analyzer (N5230A, Agilent), signal analyzer (FSV40, R&S) and power meters (AV2433, the 41st Institute of CETC), respectively. Water-cooled dummy loads absorb the output and reflected microwave power.

B. Experiments and Discussion

The ripples of the anode power supply are measured when a load, i.e., the magnetron, is producing reasonable output power. The effects of the anode voltage ripples on the magnetron's performance are then investigated. The operating anode voltage and current are maintained at 10.4 kV and 2.21 A, respectively. Fig. 4 compares the anode voltage ripple variations of the magnetron with various values of capacitance C_f. The AC component of anode voltage is operating at ~ 50 kHz, which is the same as the operating frequency of the switch supply. It is clear that improved filtering reduces the ripple. While C_f increases, the ripple gradually decreases. The peak-to-peak value of the ripple decreases from 434.4 V to 61.4 V, which also represents a drop in the ripple from 4.2% to 0.6%. Furthermore, the ripple inhibition effect is inconspicuous when C_f is higher than 0.2 μF. Therefore, we select four ripples with values of 4.2%, 1.7%, 0.9% and 0.6% for further investigation.

Then, the phase-locked bandwidths are also measured. As shown in Fig. 5, the normalized locking bandwidth characteristics with the various anode voltage ripples and injection ratios are evaluated and presented. The injection power P_{in} is tuned from 10.0 W ($\rho = 0.025$) to 180.0 W ($\rho = 0.105$) at intervals of 10.0 W. When the anode voltage ripple effects are considered, the phase locking only occurs at low injection power (< 30.0 W) when the initial anode voltage ripple is less than 2.0%. In contrast, with a high injection power at 180.0 W, the magnetron driven using the optimal voltage presents a nearly tripled locking bandwidth (3.95 MHz) when compared with the original phase-locked bandwidth (1.34 MHz).

Fig. 6 (a) illustrates that the spurious power of the phase-locked magnetron is recycled into the locking frequency at 2.4475 GHz. The peak of the spectral intensity has also risen by approximately 0.9 dB, which also agrees well with the theoretical predictions. Fig. 6 (b) shows the measured phase jitter of the phase-locked magnetron at approximately 0.1 s. The peak-to-peak value of the injected signal was nearly constant (at less than 0.3°) and the phase fluctuation decreased from ± 1.83° (original state) to ± 0.9° (ripple-suppressed state).

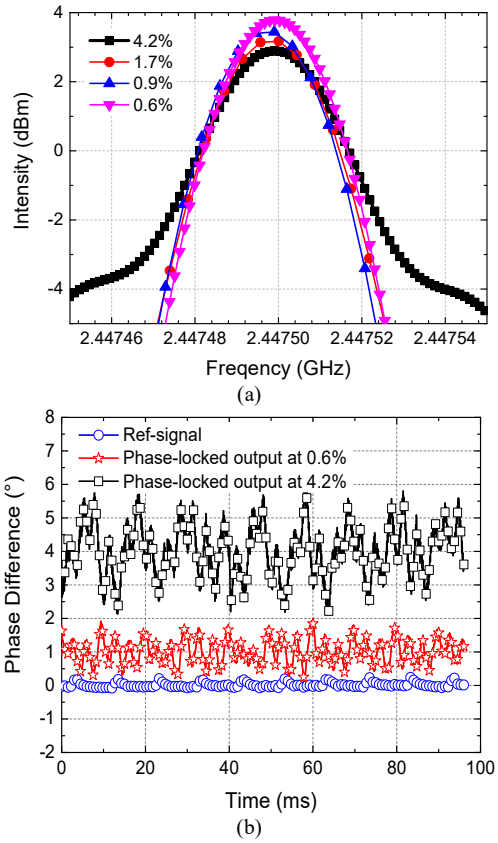

Fig. 6. Max-hold spectra (a) (Both RBW and VBW are 30 kHz.) and phase jitters (b) with respect to the various anode voltage ripples.

According to our investigated results and the consideration of cost, the SETUP of the anode voltage ripple parameter should depend on different application occasions. On the occasions of microwave heating, the magnetron does not require a high output purity which the anode ripple parameter can be approximately set as 5.0%. On the occasions of phase-controlled applications, e.g. the SSPS (Space Solar Power Station) source array or driving a superconducting radio-frequency cavities of a particle accelerator, which the anode ripple parameter should be lower than 1.0% for higher output purity and precise phase control.

IV. Conclusion

A large-power injection-locked magnetron with the anode voltage ripple inhibition was theoretically and experimentally investigated. The enhancement of injection-locking properties of a 20-kW magnetron was presented when the quality of anode voltage was optimized, i.e. the anode voltage ripple is varied from 4.2% to 0.6%. Under the circumstance of the improved anode voltage ripple, the magnetron could be more easily locked by lower injection ratio and a nearly tripled locking bandwidth was observed. Also, at the locking frequency, the spurious energy recycling phenomenon was demonstrated by achieving a higher spectral intensity and a lower phase jitter. Moreover, our investigations indicate a method to develop a high-power but low spurious noise magnetron source.

Acknowledgement

The China Scholarship Council 201906240240 and the China 973 program 2013CB328902 supported the work of Xiaojie Chen.

References

[1] W. C. Brown, “Status of the microwave power transmission components for the solar power satellite,” *IEEE Trans. Microwave Theory and Techniques*, vol. 29, no. 12, pp. 1319–1327, Dec. 1981.

[2] R. Roy, D. Agrawal, J. Cheng, et al. “Full sintering of powdered-metal bodies in a microwave field,” *Nature*, vol. 399, pp. 668–670, Sep. 1999.

[3] A. S. Gilmour, *Klystrons, traveling wave tubes, magnetrons, crossed-field amplifiers and gyrotrons*, Beijing, China: National Defense Industry Press, 2011.

[4] T. Mitani, N. Shinohara, H. Matsumoto et al. “Noise-reduction effects of oven magnetron with cathode shield on high-voltage input side,” *IEEE Transactions on Electron Devices*, vol. 53, no. 8, pp. 1929-1936, Jul. 2006.

[5] V. B. Neculaes, M. C. Jones, R. M. Gilgenbach, et al. “Magnetic perturbation effects on noise and startup in DC-operating oven magnetrons,” *IEEE Transactions on Electron Devices*, vol. 52, no. 5, pp. 864-871, Apr. 2005.

[6] N. Shinohara. “Beam control technologies with a high-efficiency phased array for microwave power transmission in Japan”. *Proceedings of the IEEE*, vol. 101, no. 6, pp. 1448-1463, Apr. 2013.

[7] A. C. Dexter, G. Burt, R. G. Carter, et al. “First demonstration and performance of an injection locked continuous wave magnetron to phase control a superconducting cavity,” *Physical Review Special Topics - Accelerators and Beams*, vol. 14, no. 3, id. 032001, pp. 1-11, Mar. 2011.

[8] B. Yang, T. Mitani, N. Shinohara. “Evaluation of the Modulation Performance of Injection-Locked Continuous-Wave Magnetrons,” *IEEE Transactions on Electron Devices*, vol. 66, no. 1, pp. 709-715, Jan. 2019.

[9] Z. Liu, X. Chen, M. Yang, et al. “Experimental Studies on a Four-way Microwave Power Combining System Based on Hybrid Injection-Locked 20 kW S-Band Magnetrons,” *IEEE Transactions on Plasma Science*, vol. 47, no.1, pp. 243-250, Jan. 2019.

[10] R. Adler, “A study of locking phenomena in oscillators,” *Proc. IEEE*, vol. 61, no. 10, pp. 1380–1385, Oct. 1973.

[11] W. Woo, J. Benford, D. Fittinghoff, et al. “Phase locking of high-power microwave oscillators,” *J. Appl. Phys*., vol. 65, pp. 861-866, Sep. 1988.

[12] H. Huang, K. Huang, C. Liu. “Experimental Study on the Phase Deviation of 20-kW *S*-band CW Phase-Locked Magnetrons,” *IEEE Microwave and Wireless Components Letters*, vol. 28, no. 6, pp. 509-511, Jun. 2018.